Research Article

Pseudoalteromonas spongiae - induced biomineralization on Q235B and 2507 steel for corrosion and biofouling resistance

Yi Zhang[1], Zhenmei Sun[1,*], Jiaxu Li[1], Xinyuan Wan[2], Gang Zhou[3], Canrong Lian[1], Rui Zhang[1], Jinlin Lu[1], Jinwen Zhang[1], Yansheng Yin[1,*]

[1]Guangdong Provincial Key Laboratory of Nanhai Microbial Mineralization Technology and Application, Institute of Advanced Materials, Guangzhou Maritime University, Guangzhou 510725, Guangdong, China.

[2]State Grid Fujian Electric Research Institute, Putian Coastal Atmospheric Environment Material Corrosion and Electric Power Equipment Safety Observation and Research Station of Fujian Province, Fuzhou 350007, Fujian, China.

[3]Guangdong Provincial Key Laboratory of Microbial Culture Collection and Application, State Key Laboratory of Applied Microbiology Southern China, Institute of Microbiology, Guangdong Academy of Sciences, Guangzhou 510070, Guangdong, China.

[*]**Correspondence to:** Zhenmei Sun, Yansheng Yin, Guangdong Provincial Key Laboratory of Nanhai Microbial Mineralization Technology and Application, Institute of Advanced Materials, Guangzhou Maritime University, Guangzhou 510725, Guangdong, China. E-mail: sun1120817625@163.com; ysyin@shmtu.edu.cn

How to cite this article: Zhang Y, Sun Z, Li J, Wan X, Zhou G, Lian C, Zhang R, Lu J, Zhang J, Yin Y. *Pseudoalteromonas spongiae* - induced biomineralization on Q235B and 2507 steel for corrosion and biofouling resistance. *Microstructures* 2026;6:[Accept]. http://dx.doi.org/10.20517/microstructures.2025.172

Received: 22 December 2025 | **Revised:** 12 March 2026 | **Accepted:** 18 March 2026

Abstract

The biomineralization process was initiated by bacteria recruiting mineral ions, the biomineral layers was formed spontaneously on metal surfaces, it influenced the service life of metal. We found that *P. spongiae* induced biomineralization layer formation on Q235B carbon steel and 2507 duplex stainless steel in bacterial suspension, and evaluated anti-corrosion and anti-fouling performance of mature biomineralization in simulated seawater. On Q235B, higher surface reactivity yielded a uniform, dark-gray, super hydrophilic biomineralization layer with minor iron oxides. It increased interfacial/charge-transfer resistance, suppressed corrosion, and reduced the attachment of *Phaeodactylum tricornutum*. On 2507, the native passive barrier limited nucleation, producing Ca–Mg carbonate deposits with exposed metal and faster charge transfer. Nonetheless, the hydrophilic protective layer still reduced biofouling in artificial seawater. Overall, *P. spongiae*–mediated biomineralization was substrate-dependent with dual anti-corrosion and anti-fouling capacity on carbon steel. On 2507, the heterogeneous biomineralization layer, while reducing biofouling, locally compromised the integrity of the passive film, resulting in pitting corrosion.

Keywords: Biofilm, *Pseudoalteromonas*, corrosion, biofouling, Q235B, 2507

Graphic Abstract

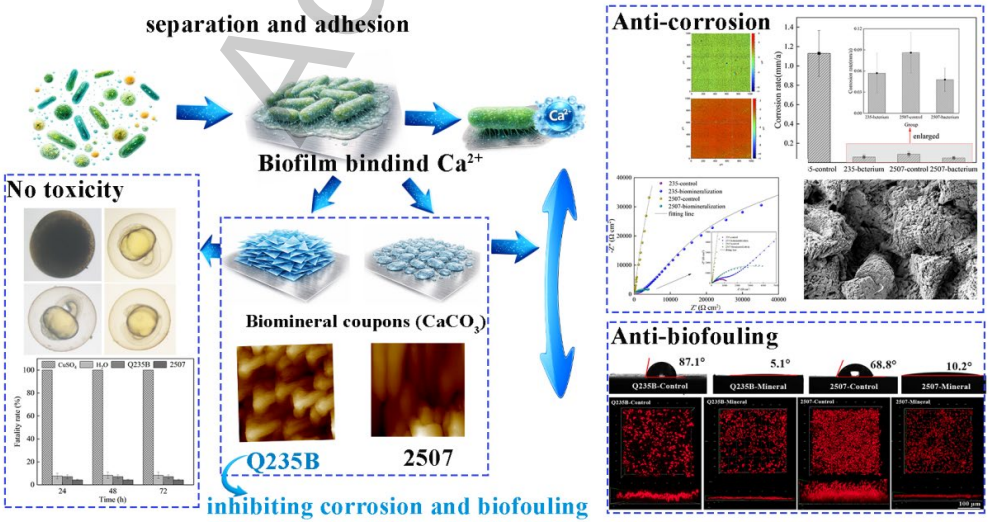

INTRODUCTION

Metals used in offshore equipment operated continuously in high-salinity seawater and were prone to chemical and electrochemical attack, degrading performance and shortening service life. In particular, chloride ions (Cl^-) promoted localized corrosion which possibly perforated the metallic materials of ships, platforms, and sub-sea pipelines. Common marine alloys–copper, carbon steel, and high-manganese steels were all susceptible to corrosion in seawater, resulting in major economic losses and safety risks [1–3]. Meanwhile, coastal eutrophication caused by industrial activities fuels promotes the bacteria and algae blooms, whose metabolites improves the formation of complex biofilms. the microorganisms, algae, and barnacles co-existed and stabilized the community (marine biofouling) [4]. Biofilms established oxygen gradients at the metal–water interface to accelerate electrochemical corrosion [5] and increased hydrodynamic drag (raising fuel consumption and CO_2 emissions) [6]. In addition, some organisms in biofilm can damage protective coatings through surface attack or delamination [7]. Q235B carbon steel and 2507 duplex stainless steel were widely used in marine, but both still corroded under harsh conditions [8, 9], microbial metabolites within biofilms can further initiate localized corrosion on Q235 and 2507 surfaces [10, 11]. Historically, tributyltin (TBT) coatings provided strong biofouling resistance, but their ecological and human toxicity in marine were unacceptable, highlighting the urgent need for environmentally friendly strategies [12]. In recent years, some marine microorganisms could play dual roles in mitigating corrosion by secreting extracellular polymeric substances (EPS) that chelate Ca^{2+}/Mg^{2+} to form the protective biomineralization on metal surfaces. These biomineralized layers offered a promising green route to coupled inhibit corrosion and biofouling.

Biomineralization proceeded via two pathways: biologically controlled mineralization (BCM) and biologically induced mineralization (BIM). BIM refers to the process that bacteria recruited mineral ions through altering environmental conditions, such as pH, carbonate alkalinity, redox [13], it was the dominant routine for forming biomineral

layers on metal surfaces. Some microbes could produce uniform, adherent biomineral coatings that were environmentally friendly and conformed to complex surfaces, serving as protective barriers from corrosion. Previous studies highlighted this conclusion, Liu et al. showed that *P. lipolytica* secreted bacterial cellulose polysaccharides, which induced calcite precipitation and protected steel substrates [14], the cellulose polysaccharides regulated biomineralization process via biofilm [15]. Guo et al. also proposed the molybdenum increased the adhesion of *Bacillus subtilis* on the material surface and improved the biomineralization ability [16], his earlier research indicated that biomineral layers induced by *B. subtilis* would inhibit the *Vibrio* natriegens-induced corrosion in seawater [17]. Similarly, methanogens driven carbonate deposition on Dutch metal dikes produced dense biomineral layers that prevented corrosion for about 50 years [18]. Notably, *Shewanella putrefaciens* has been used to restore the damaged epoxy coatings and to suppress corrosion on carbon steel [19]. Overall, extensive studies have confirmed that biomineral coatings could significantly mitigate metal corrosion [20, 21]. The corrosion protection mainly arose from (i) microbial metabolic activity consumed dissolved oxygen at the biofilm and metal interface, resisting oxygen gradients that drove electrochemical corrosion; (ii) physical barriers effectively limited the direct contact between corrosive agents and substrates [22]. There had some methods to prevent corrosion, the sacrificial anodes, cathodic protection systems, and chemical coating were well-established corrosion-control strategies [23-25]. There still have some limitation, including finite service life [26], uneven potential control, and environmental concerns. In addition, biofouling still remained a pressing challenge in marine, it would be combined with bacteria to accelerate metallic corrosion [27, 28]. It was particularly crucial to produce an integrated dual inhibiting corrosion and biofouling coating. Biomineralization offers a promising sustainable routine to develop the protective coating, some marine bacteria such as *Alteromonas*, *Pseudoalteromonas*, and *Pseudomonas* exhibited high mineralization capacity, making them strong candidates for green, durable anticorrosion and antibiofouling strategies[29–31]. Previous studies on bacteria-induced biomineralization have mainly focused on corrosion mitigation,

while substrate-dependent film nucleation, growth, and coverage have been less addressed. For carbon steel versus duplex stainless steel, the roles of substrate reactivity and passive films in governing film continuity and protection remain undercompared.

Pseudoalteromonas is a genus of Gram-negative bacteria widely distributed in seawater, it has remarkable metabolic capability and strong environmental adaptability [32]. *Pseudoalteromonas* spp. have become model organisms in biofilm and biomineralization research due to they secreted numerous extracellular polymeric substances (EPS) during growth [33, 34]. Their metabolic byproducts could modulate the local environmental, particularly pH and ion concentrations, thereby promoting the formation of continuous and dense biomineralized layers on metal surfaces [35, 36]. In this study, *Pseudoalteromonas. spongiae* was isolated from the coastal waters near Guishan Island in the South China Sea, under conditions of approximately 22 °C and 30 ‰ salinity. In this study, the biomineralization behavior induced by P. spongiae on Q235B carbon steel and 2507 duplex stainless steel was investigated, with particular focus on the corrosion resistance and antifouling performance of the formed biomineralized layers in artificial seawater. The work aims to clarify the substrate-dependent characteristics of biomineral layer formation and to evaluate the potential of this biomineralization strategy for marine metal protection.

MATERIALS AND METHODS

Bacterial culture and steel

The bacterial strain used in this study was isolated from seawater collected near Guishan Island (South China Sea). After purification and taxonomic identification, phylogenetic analysis revealed that the isolate shared the highest similarity with *Pseudoalteromonas spongiae UST010723-006* by 16S rRNA. It was grown in 2216 E broth (Hopebio, Qingdao, China), containing 37.4 g/L powder in deionized water and autoclaving at 121℃ for 20 min. After cooling to room temperature, sterile $NaHCO_3$ (UV-sterilized) was added to achieve a final concentration of 1.8 g/L. The solid

medium consisted of 2216 E and agar (Hopebio, Qingdao, China). Bacterial suspensions were incubated at 22 °C with shaking at 120 rpm, then were spread on agar plates, the single colony morphology was examined under a stereo microscope (MDJ200, China). Optical density at 600 nm (OD_{600}) of bacterial suspension was measured using a micro plate reader (arioskan LUX, Singapore), the initial bacteria (1 mL, OD_{600} = 0.1) was inoculated into 200 mL 2216 E broth for the immersed experiment.

The Q235B carbon steel used in this study had the following chemical composition (wt.%): 0.7 Mn, 0.35 Si, 0.045 P, 0.045 S, 0.22 C, with the balance being Fe . The chemical composition of 2507 duplex stainless steel (wt.%) was: 24.0–26.0 Cr, 6.0–8.0 Ni, 3.0–5.0 Mo, 0.2–0.3 N, 1.2 Mn, 0.8 Si, 0.035 P, 0.02 S, 0.03 C, with the balance being Fe, They are from Shenzhen Dinglong Industrial Materials Co., Ltd. Both steels were cut into rectangular coupons (10 × 10 × 5 mm), sequentially ground with SiC papers (120–1000 grit), The polished samples were then ultrasonically cleaned in anhydrous ethanol to remove any surface contaminants, air-dried, and sterilized under ultraviolet (UV) irradiation for 30 min. The UV-sterilized Q235B and 2507 coupons were immersed in bacterial suspensions and sterile medium for subsequent experiments. The pH of bacterial suspensions was monitored daily for 8 days using a pH meter (Sartorius PB-10, Germany). Viable bacteria were enumerated by serial dilution and spot-plating on agar plates containing nutrition with triplicate for each group.

Properties of the surface mineral layer on Q235B and 2507

During the period of Q235B and 2507 coupons immersed in bacterial suspension, samples were retrieved after 3, 5, and 7 days, gently rinsed with deionized water, air-dried, and photographed to record the morphology of the biomineralized layer. The phase composition of the samples immersed for 7 days was analyzed by X-ray diffraction (SmartLab, Japan) over a 2θ range of 10–80° at a scanning rate of 5° min^{-1}, datasets were processed with Jade software. Separately, the samples immersed after 7

days were rinsed three times with deionized water, dried at 40 °C for 24 h and then subjected to contact-angle measurements to evaluate the hydrophilicity of the biomineralized layer. The polished (1000-grit SiC) Q235B and 2507 without immersion served as blank controls, all measurements were performed in triplicate.

Microscopic morphology of both substrate

The 7-day immersed samples were fixed in 2.5% glutaraldehyde for 15 min, then dehydrated in graded ethanol (30, 40, 50, 60, 70, 80, 90, and 100 vol%; 10 min). The coupons were sputter-coated with Pt using a vacuum coater (nanoPVD S10A, UK; 30 mA, 60 s) after air-dried at room temperature. The micro structure of the biomineralized layer was examined using a focused ion beam scanning electron microscopy (FIB–SEM; Crossbeam 350, Germany), the cross-sectional morphologies of the biomineralized layer were obtained by FIB milling. Elemental composition and distribution on coupons were analyzed by energy dispersive spectrometer (EDS; ZEISS SmartEDX, Germany).

Corrosion behavior during biomineralization formation

Samples were welded to copper wires and embedded in epoxy resin, leaving a defined working area exposed (1 cm^2), they were immersed in bacterial suspensions with the initial inoculum (1 mL, OD_{600} = 0.1) and sterile medium as the experimental and control group, respectively. In situ electrochemical impedance spectroscopy (EIS) was performed using a three-electrode systems, with the sample as working electrode, saturated calomel electrode as reference, platinum plate as counter electrode. Measurements were carried out on an electrochemical workstation (Parstat IM6e, Princeton Applied Research, USA). A 10 mV sinusoidal perturbation was applied at the open circuit potential (OCP) with 300 s, the frequency range was 10^{-2}–10^5 Hz. The EIS was measured after 3 and 7 days of immersion, the EIS of mature biomineralized layer was measured after 7 days of immersion in room temperature environment. The EIS data was fitted and analyzed using ZSimpWin.

The corrosion rate of the samples was calculated using the following equation:

$$V_{corr} = (87600 \times \Delta m)/\rho A t \quad (1)$$

where, V_{corr}、t、ρ、A and Δm represented the corrosion rate (mm/a), immersed time (h), steel density ($g \cdot cm^{-3}$), exposed area (cm^2), and mass loss (g), respectively. Steel samples were immersed in different bacterial suspensions for 7 d at 22 °C (initial inoculum as above). After immersion, samples were sequentially rinsed with concentrated hydrochloric acid, saturated $NaHCO_3$ (China National Medicines Corporation Ltd.), and deionized water, air-dried, and then examined with a white light interferometer (Bruker ContourGT, Germany) to assess the pitting corrosion morphology.

Biofouling influence of mature biomineralized layer

The mature biomineralized layer was made by coupons immersed in bacterial suspension aferr 7 days. The adhesion assays were performed in 24-well polypropylene plates (Corning, USA), the bacterial suspension (2.0 mL, OD_{600} = 0.1) were added in each well and incubated statically at 22 °C. After incubation, suspension was discarded, and wells were rinsed three times with deionized water to remove non-adherent bacteria. The adhesive biomass were stained with 1 wt. % crystal violet (2.0 mL per well, 15 min), the wells were rinsed thoroughly with deionized water until the blank control wells were colorless. After dried, the bound dye was solubilized with ethanol, and absorbance was measured at 550 nm was recorded (blank subtraction), all experiments were performed in triplicate.

To investigate capacity to inhibit biofilm of mature biomineralized layer, Q235B and 2507 with biomineralization were subsequently immersed in *Vibrio chagasii* suspension for 7 d. A staining solution was prepared by mixing 3 μL SYTO 9 Green fluorescent nucleic acid stain and 3 μL propidium iodide (PI) in 1 mL PBS. Steel coupons were removed from the bacterial suspension, placed in a sterile petri dish,

and gently rinsed three times with sterile PBS to remove non-adherent bacteria. Subsequently, 200 μL of the staining solution was added and incubated at room temperature in the dark for 20 min. Samples were rinsed with sterile PBS to remove excess dye, air-dried in the dark, and imaged with a confocal laser scanning microscopy (LSM 900, ZEISS, Germany) to assess biofilm viability and structure.

The diatom attachment is a common initial step in marine biofouling development, the antibiofouling in marine in this manuscript in this work refers to inhibition of microfouling, mainly bacterial biofilm formation and early-stage diatom attachment. To simulate algal attachment under marine conditions, the artificial seawater (ASW composition in Table 1) was prepared, supplemented with *P. tricornutum* (4.1×10^6 cells/mL) and *V. chagasii* (10^4 cells/mL). Q235B and 2507 coupons with biomineralized layers, as well as bare control were immersed in the above system, and the attachment of diatoms on the substrate surface was documented photographically. Owing to the auto fluorescence of algal pigment, CLSM (e^x/e^m = 647/680 nm) was used to observe the diatom attachment on substrate surfaces.

Corrosion resistance of mature biomineral layer

Q235B and 2507 coupons embedded in epoxy resin were immersed in bacterial suspensions for 7 d to form a biomineral layer. After retrieval, superficial biofilm was removed with 75% ethanol, samples were air-dried and then immersed in ASW for 3 d, which containing NaCl 23.50, MgCl •$6H_2O$ 10.78, Na_2SO_4 3.92, $CaCl_2\cdot2H_2O$ 1.47, KCl 0.66, $NaHCO_3$ 0.20, H_3BO_3 0.10, $SrCl\cdot6H_2O$ 0.025, NaF 0.003. EIS was performed as in Section 2.4, except the electrolyte was replaced with ASW.

Zebrafish embryo toxicity of biomineral coupons

Ten biomineral Q235B coupons (10 × 10 × 5 mm) with bacteria removed were gently rinsed to 500 mL of sterile deionized water (DI). In parallel, ten 2507 duplex stainless-steel coupons (10 × 10 × 5 mm) with a biomineralized layer were immersed in 500 mL of sterile deionized water. All vessels were sealed and incubated statically

in the dark at 25±1℃ for 14 days to obtain leachates. No solution replenishment or replacement was performed during the leaching period. After leaching, the solutions were collected and used immediately as test media. Zebra fish embryos were exposed to the leachates in 24-well plates, with one embryo per well in 2 mL of test solution. For each treatment, 30 wells (n = 30 embryos) were used. Sterile DI water served as the negative control, while 10 μM $CuSO_4$ was used as the positive control. Embryo survival and gross developmental outcomes were assessed over a 3 d exposure period.

Statistical analysis

Data analysis was conducted using SPSS 19.0 . One-way analysis of variance was applied to determine differences between experimental groups. Results are reported as the mean ± standard deviation. Significance levels were set at *p < 0.05, **p < 0.01, and ***p < 0.005

RESULTS AND DISCUSSION

Growth and metabolic conditions of bacteria

The 8-day growth trajectory of *P. spongiae* was shown in Fig 1a. During 48 h, the results exhibited an exponential phase, with bacterial concentration rapidly from ~ 5.0 × 10^5 to ~ 2.5 × 10^9 cells/mL. The accompanying pH changes of bacterial suspension during this period were presented in Fig 1b, As an aerobic bacterium, *P. spongiae* led a slight pH decrease during rapid proliferation, consistent with the production of acidic metabolites. In agreement with this result, Kim *et al.* reported that EPS secreted by *P. elyakovii* isolated from the Arctic Ocean was enriched in –COOH groups that ionize to release H^+ and acidify the medium [37].

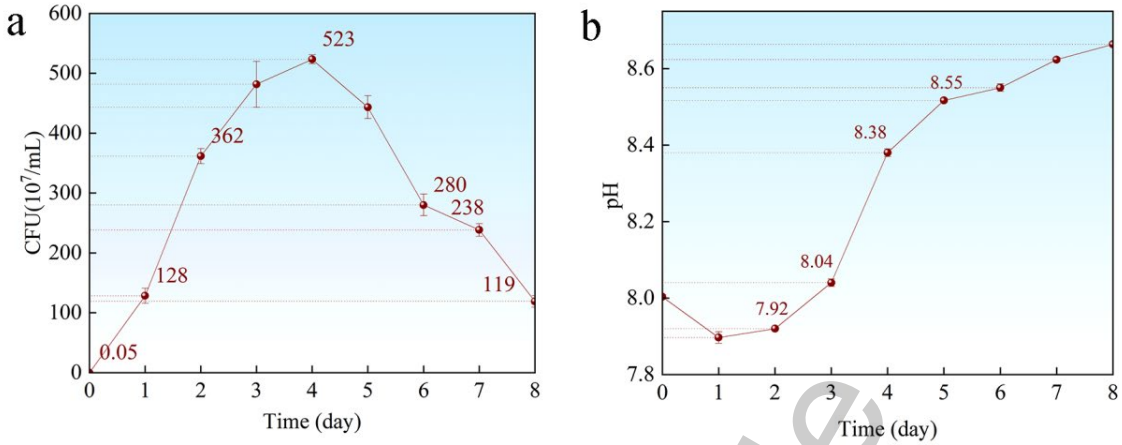

Fig 1. (a) Time dependence growth curve of bacteria and (b) the pH curve during 8 days

Additionally, Respiratory CO_2 may further contribute to this modest pH decline. Subsequently, *P. spongiae* entered the stable period when bacteria proliferation slowed significantly (2-4 d) accompanied with accumulation of metabolic products. The pH rose from ~7.92 to ~8.55, representing the steepest pH ascent observed (Fig. 1b). After 4 d , cell death commenced gradually, nevertheless, bacterial concentrations remained above 10^9 cells/mL throughout 2-7 d. Overall, the pH of bacterial suspension increased steadily, but the increasing rate slowing markedly after 5 d (Fig. 1b). Taken together, these results indicated that at 22℃ in a 200 mL nutrient-rich medium, *P. spongiae* completed a full growth cycle within approximately one week, accordingly, the 7-day experimental period was adopted for this study.

The surface characteristics of the biomineralized layer

During the process of biomineral layers formation, the metal surface progressively lost its metallic luster and developed a matte coating. The macroscopic appearance of coupons immersed in the bacterial suspension was shown in Fig 2a, *P. spongiae* produced biomineralized layers with distinct coloration on Q235B and 2507. A dark gray layer formed on Q235B, whereas a comparatively lighter layer formed on 2507, with the contrast most pronounced during 5 d. The compositional analysis revealed that calcium carbonate was the predominant constituent of the biomineralized layers

on both substrates (Fig 2b). However, the coating on Q235B also contained some iron oxides, it indicated that partial dissolution and $Fe^{2+/3+}$ releasing of the carbon steel during the biomineralization reaction which subsequently imparting the darker product. Some reported that mild substrate corrosion, by elevating Fe^{2+} concentrations, could enhance bacteria induced carbonate deposition to form the biomineral layers, it was possibly conducive to form the nucleation sites of biomineralization [22].

Fig 2c showed the hydrophilicity of bare substrates and their biomineralized coatings. The static contact angles of bare Q235B and 2507 were ~ 87.1° and ~68.8°, respectively, consistent with moderately hydrophilic surfaces. In contrast, the contact angles of biomineralized layers decreased to ~ 5.1° and ~ 10.2°, awarding the coatings hydrophilic properties. Unlike the conventional inhibiting corrosion strategies that emphasize super conductivity to minimize the contact between water and substrate [38, 39], super hydrophilic interface could sustain a continuous water layer that impeded oxygen and other corrosive species and reduced biofouling in ASW. Notably, the biomineralized layer on Q235B exhibited stronger wetting ability than that on 2507, plausibly due to a more uniform hydrophilic mineral phase.

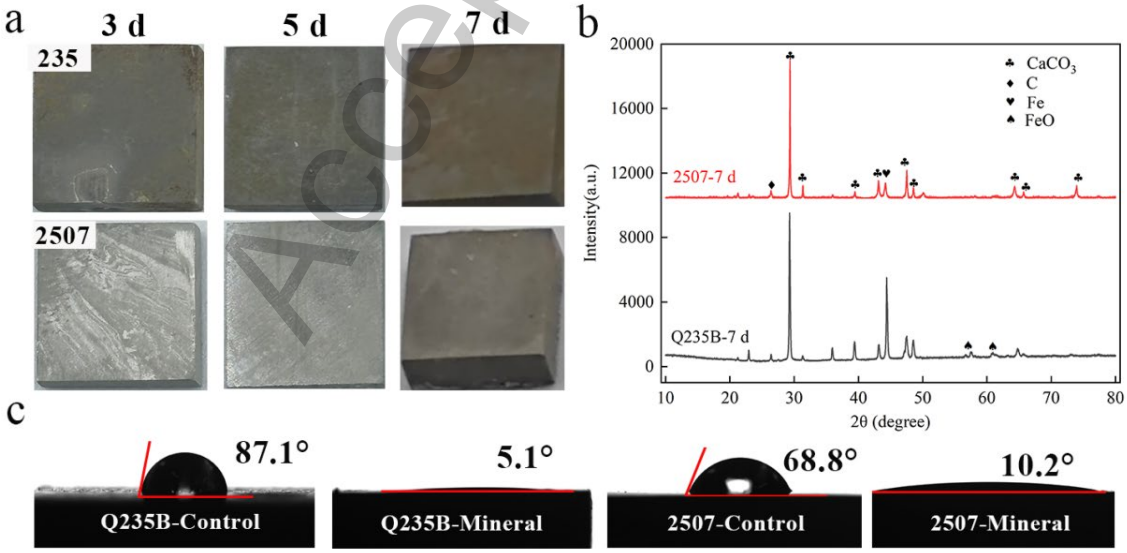

Fig 2. (a) Macro images of Q235B and 2507 during 7 days ; (b) the XRD image and (c) contact angle images of Q235B and 2507 after 7 days.

The structure of the biomineralized layer

Fig. 3a and 3b showed microscopic morphology of biomineralized layers formed on Q235B and 2507 after 7 d of immersion in *P. spongiae* suspension, respectively. On Q235B, the deposit was dominated by clumps and other irregular accretions that formed a continuous blanket on substrate, higher-magnification micro graphs resolved stacked with no discernible exposure of the underlying steel. The surface EDS indicated that C, O, and Ca as the major elements uniformly distributed minor Fe, consistent with the XRD results. Cross-sectional images further confirmed a relatively uniform, compact biomineralized coating that was well bonded to the substrate, with neither exposed metal nor internal voids (Fig 3c). AFM showed the biomineralized architectures formed on the two substrates at higher spatial resolution in Fig. 4a, the layer on the Q235B surface consisted of orderly triangular motifs ~350–400 nm in size arranged in a stacked pattern. The mean topographic relief was about 580.2 nm, exceeding that of the layer on the 2507 surface (456.4 nm), indicating that the roughness of the mineralized layer on Q235B was higher than 2507 substrate.

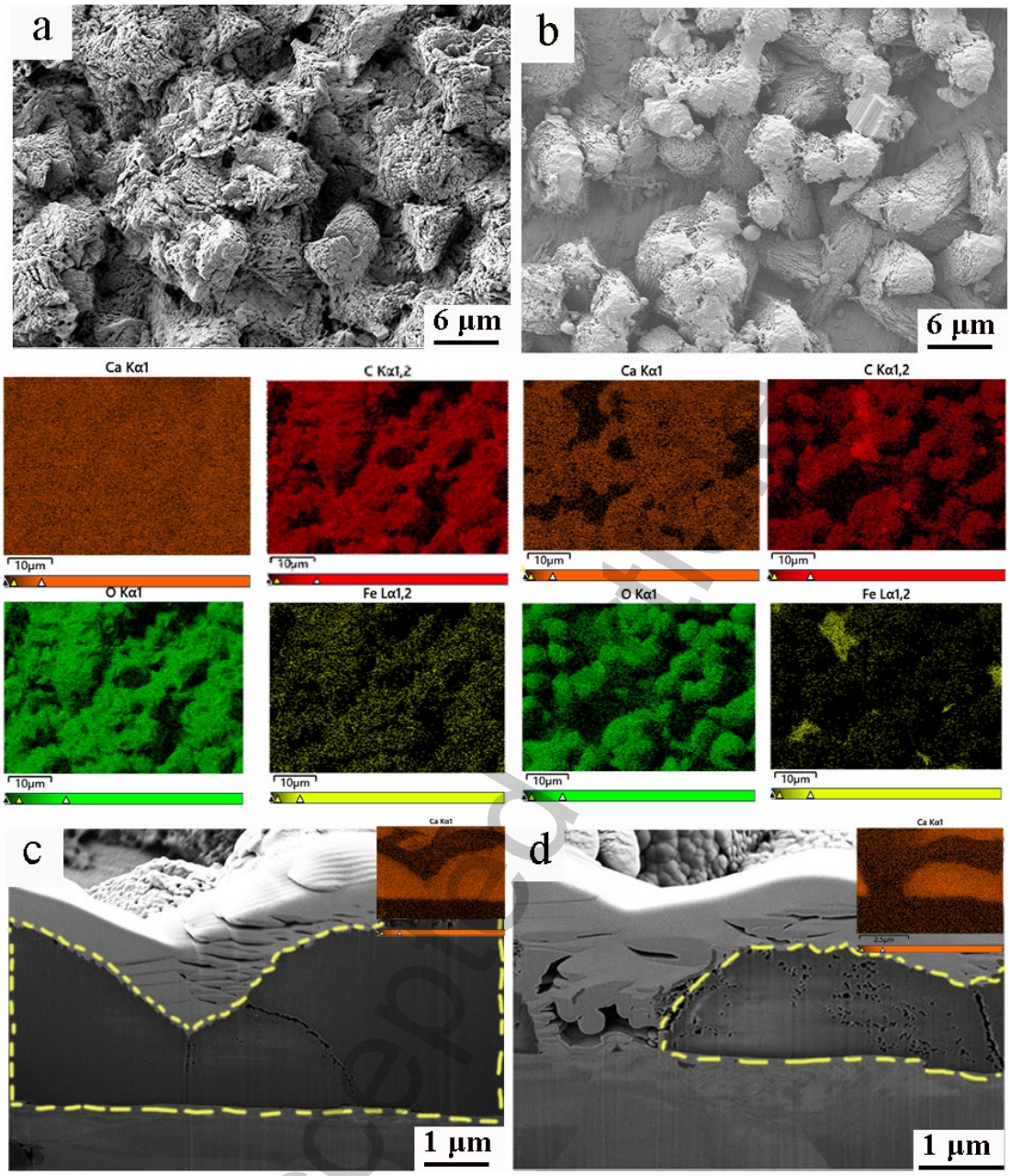

Fig 3. The SEM images of (a) Q235B and (b) 2507 with corresponding EDS images immersed in bacterial solution after 7 days; the crossing SEM images with calcium element distribution of (c) Q235B and (d) 2507 after immersion of 7 days.

In contrast, the biomineralized layer on the 2507 was spatially heterogeneous, leaving portions of the substrate uncovered. The prevalent morphology was rod-like, at higher magnification, the coating was comprised of small triangular subunits and contained pores. EDS indicated a composition similar to that on Q235B (C, O, Ca) but with localized Fe enrichment, it showed that part of the matrix was directly exposed, that

maybe induced electrochemical corrosion. FIB–SEM cross-sections highlighted two salient features of the 2507 layer, an externally discontinuous $CaCO_3$ overlayer that exposes isolated regions of steel, and a highly porous interior with a honeycomb-like architecture (Fig 3d). The nanoscale images indicated that the surface structure of 2507 was disorganized and lacked barrier efficacy toward corrosive environments (Fig 4b). In conclusion, *P. spongiae* formed biomineralized layers of various structure on two substrates with different inhibiting corrosion capacity, it was consistent with the study about the corrosion inhibition of X80 pipeline steel [40].

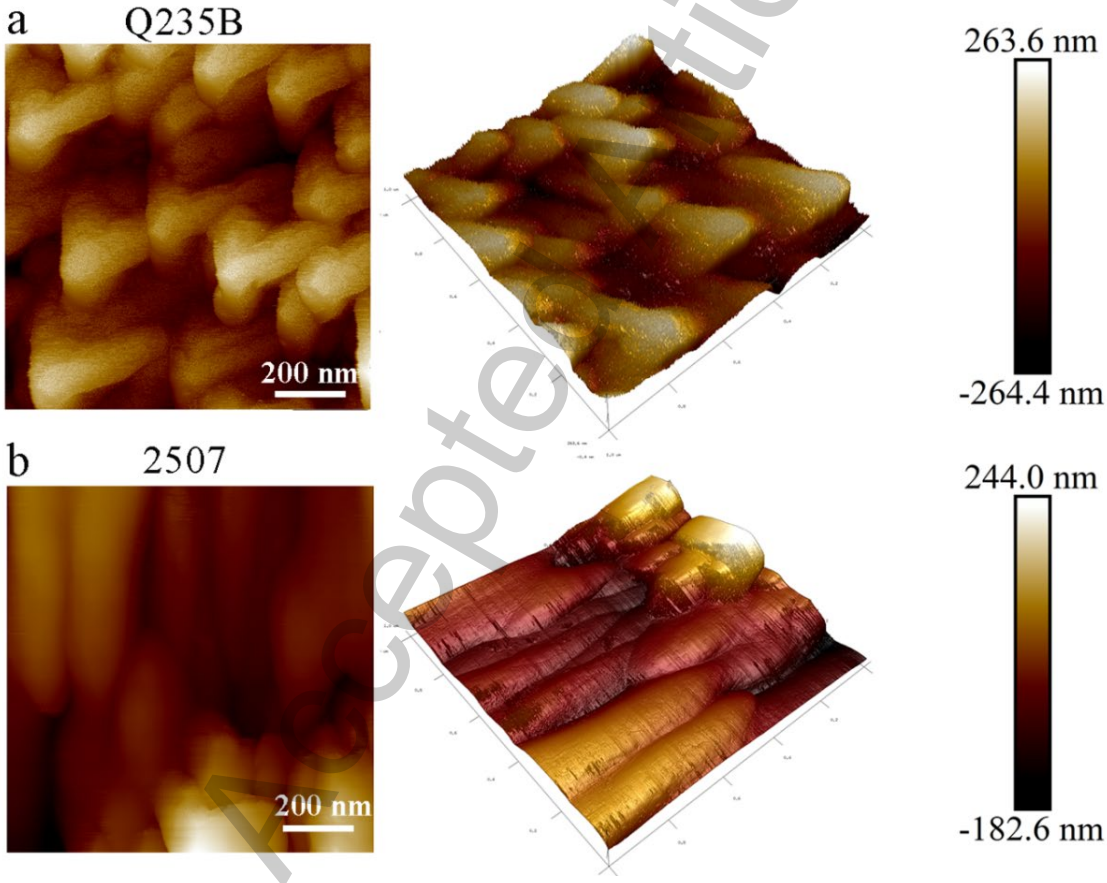

Fig 4. The AFM images of (a) Q235B and 2507 immersed in bacterial suspension after 7 days.

Corrosion behavior of the substrate

Carbon steel was one of the most widely used materials, while it was prone to corrosion in seawater and atmosphere [41, 42]. The formation process of

biomineralization on Q235B provided immediate anticorrosion capacity. Fig. 5a showed the uniform corrosion rates of Q235B and 2507 immersed in bacterial suspensions after 7 d. For Q235B, the biomineralized layer reduced the uniform corrosion rate from ~1.15 mm/a in the sterile medium to ~0.06 mm/a with *P. spongiae* with approximately 20-fold decrease, it demonstrated the effective suppression of general corrosion in high-salinity environment. In addition, the protective barriers also inhibited localized attack and pits, pitting corrosion was usually taken place in oil pipelines in the offshore oil industry [43]. there was no obvious pits on the exposed substrates after removing the biomineralized layer compared with the large-diameter pits on Q235B in the blank medium (Fig. 5b). By contrast, 2507 coupons retained an intact surface with no localized corrosion in both control and *P. spongiae* suspension, it was likely decided by its native Cr_2O_3 passive film with better stability [44, 45].

A relatively uniform biomineralized layer formed by *P. spongiae* on Q235B yielded an impedance response approaching ideal capacitive behavior and thereby inhibited substrate corrosion. The Q235B and 2507 Nyquist and Bode plots (Fig. 5c-f) were described by $R_s(R_fQ_f(R_{ct}Q_{dl}))$ and $R_s(R_{ct}Q_{dl})$(Fig. 6a, b). The fitting results, showed a larger capacitance than the sterile control, a higher mid-frequency phase angle during 3–7 d, and a substantial increase in film resistance (R_f). These features indicated progressive thickening of the biomineral layer and enhanced corrosion resistance of Q235B. By contrast, on 2507 duplex stainless steel the biomineral layer degraded the passive film, lowering impedance and accelerating charge transfer and corrosion. In the sterile control, the peak of EIS curve extended to low frequencies. However, in the bacterial suspension, the phase angle collapsed to a single peak centered in the middle frequency region after the formation of biomineral layer (Fig. 5e, f), the peak narrowed and the low-frequency phase angle dropped sharply, evidencing faster charge transfer and partial disruption of the passive film by a heterogeneous biomineral layer.

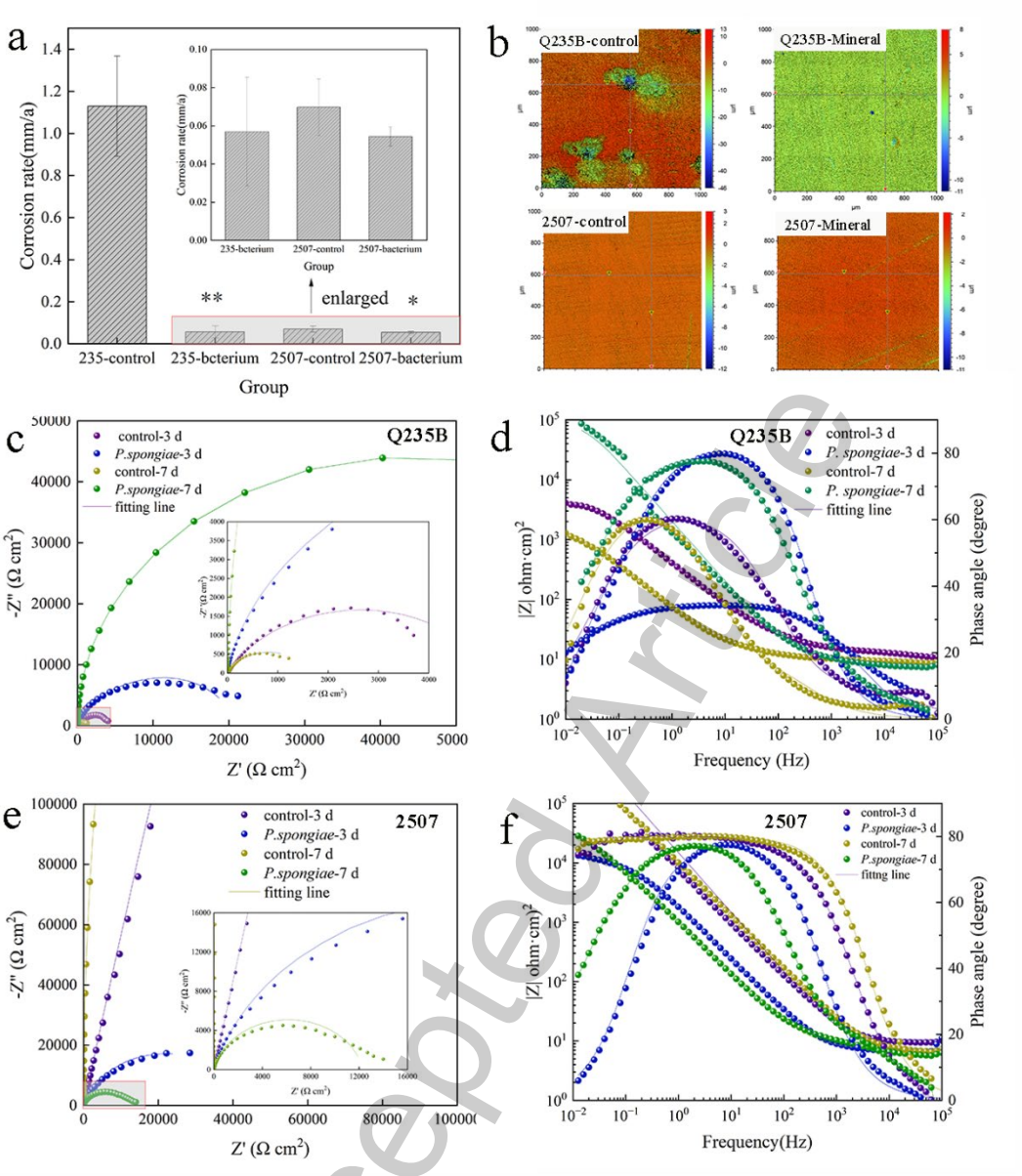

Fig 5. (a) The uniform corrosion rate, (b) localized corrosion of Q235B and 2507 after 7 days immersion, (c) Nyquist plot and (d) Bode plot of Q235B immersed in bacterial suspension during 7 days, (e) Nyquist plot and (f) Bode plot of 2507 immersed in bacterial suspension during 7 days (The error bars represent the variance of the three repeating groups. The statistical significance is *p<0.05, **p<0.01.)

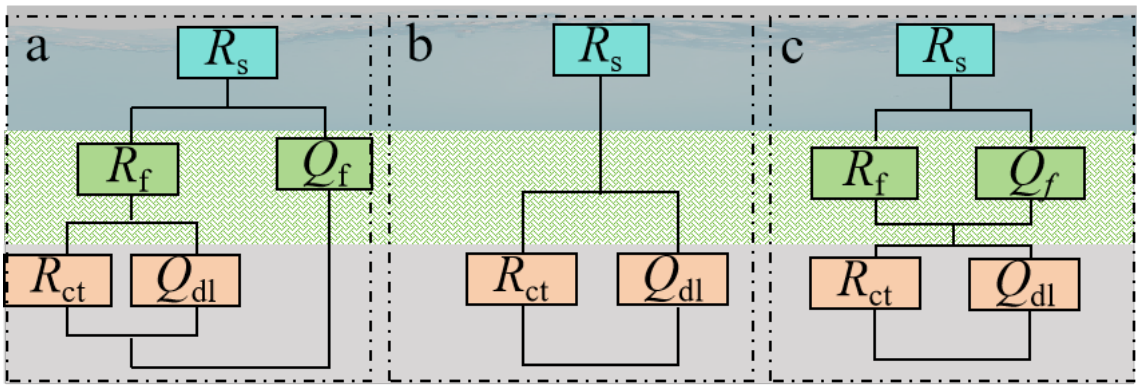

Fig 6. The equivalent circuit images used in Nyquist plots.

Table 1. Electrochemical impedance parameters fitted from the Nyquist plots (Fig 5)

Steel	Groups	R_S ($\Omega \cdot cm^2$)	Y_f ($S.s^n/cm^2$)	n	R_f ($\Omega \cdot cm^2$)	Y_{dl} ($S.s^n/cm^2$)	n	R_{ct} ($\Omega \cdot cm^2$)
Q235B	control-3 d	10.7	9.4×10^{-5}	0.7	6.6	5.2×10^{-4}	0.7	5248
	P. spongiae-3 d	7.8	1.0×10^{-4}	0.9	1.2×10^{4}	3.2×10^{-5}	0.9	8446
	control-7 d	9.3	1.3×10^{-1}	0.7	9.4	2.1×10^{-3}	0.8	1601
	P. spongiae-7 d	8.0	3.0×10^{-5}	0.9	16.7	4.7×10^{-5}	0.9	8.6×10^{4}
2507	control-3 d	10.5	/	/	/	1.1×10^{-5}	0.9	3.3×10^{6}
	P. spongiae-3 d	7.3	/	/	/	1.1×10^{-4}	0.9	1231
	control-7 d	6.9	/	/	/	1.9×10^{-5}	0.9	1.9×10^{7}
	P. spongiae-7 d	7.3	/	/	/	2.1×10^{-4}	0.8	4.5×10^{4}

3.5 The corrosion and biofouling resistance of mature biomineralized layers

Biofouling not only imposed additional economic costs but linked closely with adhesive corrosion of materials [46, 47]. To further evaluate the inhibiting biofilm capacity of biomineral layer induced by *P. spongiae*, we selected *V. chagasii* isolated from the same location as a test bacterium because of its strong adhesiveness and propensity to form biofilm on substrates (Fig. 7a). Wang et al. considered that *V. chagasii* had the wider distribution in marine likely reflecting strong competitive positions, it would have the potential biofouling damage [48]. *V. chagasii* and *P.*

spongiae are both Gram-negative, the former formed white colonies, whereas the latter appeared pale yellow (Fig 7b). Fig. 7c presented biofilm on substrate surfaces after immersion in *V. chagasii* suspension for 7 d. On the bare steel surface, a large number of live bacteria adhered at an early stage and formed a continuous biofilm, suggesting active bacterial adhesion and proliferation. On both steels, bacteria in biofilm on coupons decreased, owing to the comparatively uniform biomineral layers on Q235B, the biofilm showed no obvious porosity, bacteria would begin their death process. The mineral layer that has not been immersed in the bacterial solution, due to the fact that some dead bacteria still remain in the early bacteria-attached biominerals, serves as the control sample of the initial residual dead bacteria in the biomineralized layer. The surface results indicated that the biomineral layer still had a stable inhibitory effect on the long-term growth of biofilm. The higher magnification images revealed distinct attachment modes of *V. chagasii* on the two biomineralized substrates which was attributed to different biomineral structure. biomineralization formation could increase vertical effective stress [49], when cells are subjected to stress, alterations occur in both gene expression and cellular structure [50]. Based on the above research, it was possible that nonuniform biomineralization can produce local shear stresses to make cell death, however, further verification was still necessary.

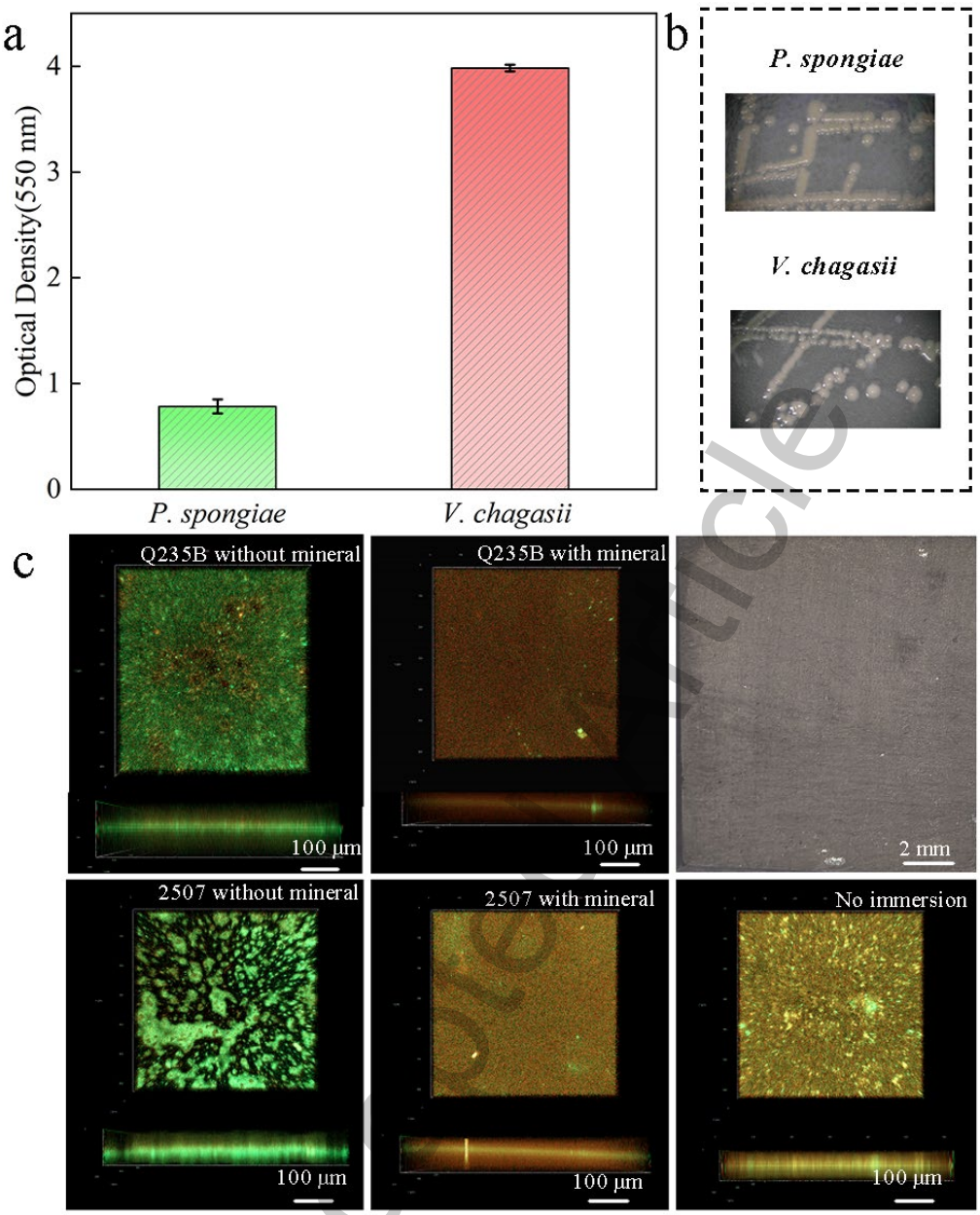

Fig 7. (a, b) The adhesive capacity and morphology of *P. spongiae* and *V. chagasii*; (c) The biofilm of *V. chagasii* on Q235B, 2507 without and with biomineral after 7 days immersion, the macroscopic view of the biomineralized layer is in the upper right corner.

To more faithfully simulate marine biofouling, we employed *V. chagasii* and the *P. tricornutum* as the model bacterium and alga, respectively to assess the inhibiting biofouling capacity of biomineralization in ASW alongside a sterile control. Fig. 8a showed the macroscopic appearance of bare coupons and coupons with mineral layer

covered immersed in ASW containing bacteria and alga. Bare Q235B corroded severely and formed a yellow rust layer, nevertheless, Q235B with a dark gray biomineral coating showed strong capacity of inhibiting corrosion, there was no visible corrosion products. The CLSM images indicated that the biomineral layer on Q235B also reduced diatoms attachment, the attached diatoms film was thinner than that on bare steel (Fig. 8b). There had no obvious corrosion products on bare 2507, but it was adhered by numerous diatoms, this result suggested that the stainless steel was more vulnerable to biofouling than carbon steel to some extent. This is likely because its surface did not release a large amount of heavy metal ions, allowing bacteria and diatoms to continue to grow, whereas stainless steel would suffer heavier biofouling than carbon steel though it could resist corrosion. The super hydrophilic mineral layer greatly protected 2507 against biofouling, diatoms attachment was reduced in both thickness and area (Fig. 8b). The biomineral layer with biofilm on surface had a better inhibitory effect on diatom attachment, there may be interspecific biological competition, which inhibits the colonization of diatoms on the surface (Fig 8c). Taken together, these results highlighted the significant role of the super hydrophilic biomineral layer in metallic anti-corrosion and anti-biofouling. It effectively limited corrosion and biofouling on carbon steel, and even a non-uniform layer could cut the attachment of biofouling organisms on stainless steel. However, the uneven biomineral layers would damage the corrosion resistance of the passivation film. biomineralization still had the potential to become a green and economical method in corrosion and biofouling inhibition with further research.

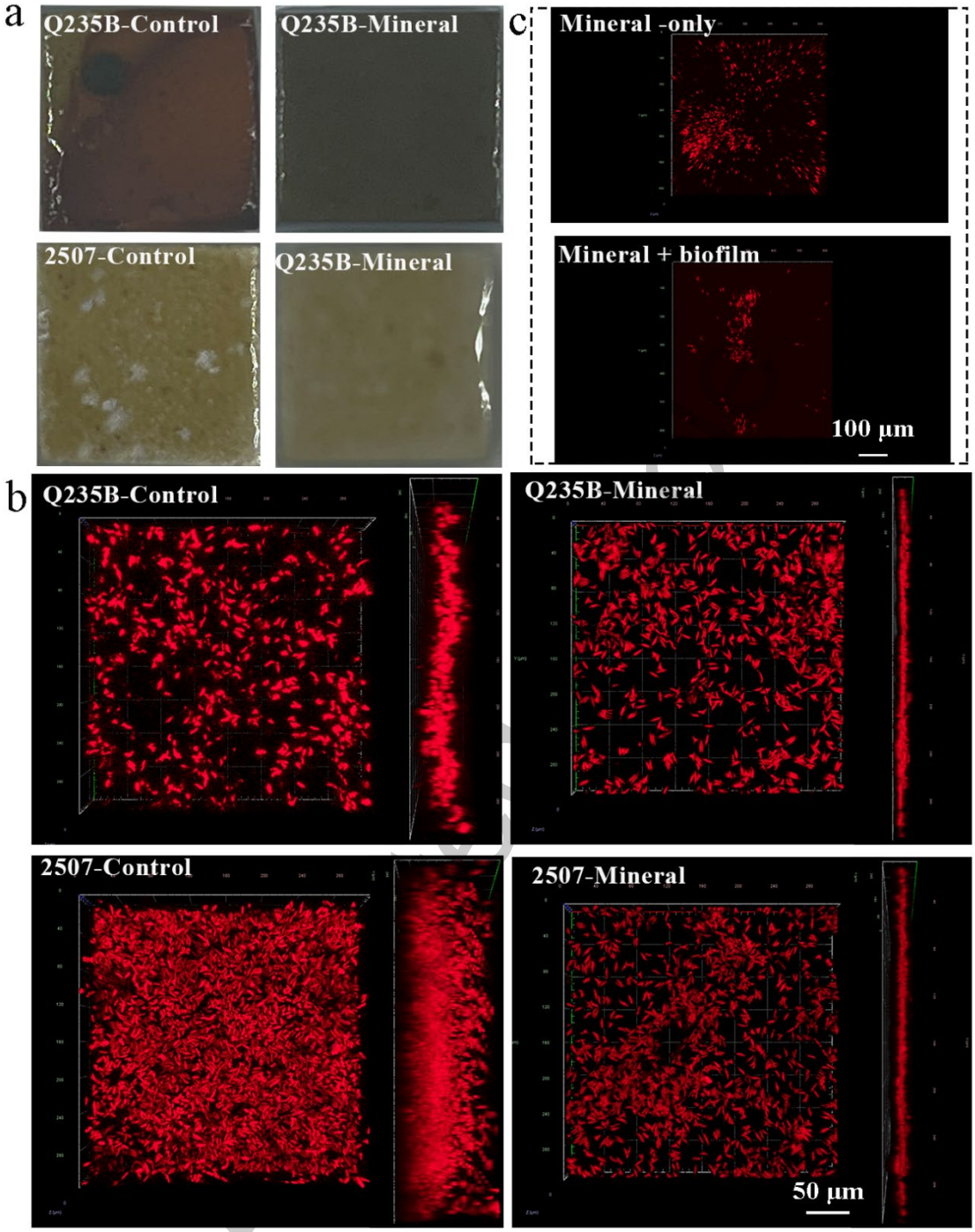

Fig. 8. (a) The macro and (b) micro images of bare Q235B, 2507 and its biomineralization (c) the biomineral Q235B without and with biofilm immersed in ASW with *V. chagasii* and *P. tricornutum* after 3 d.

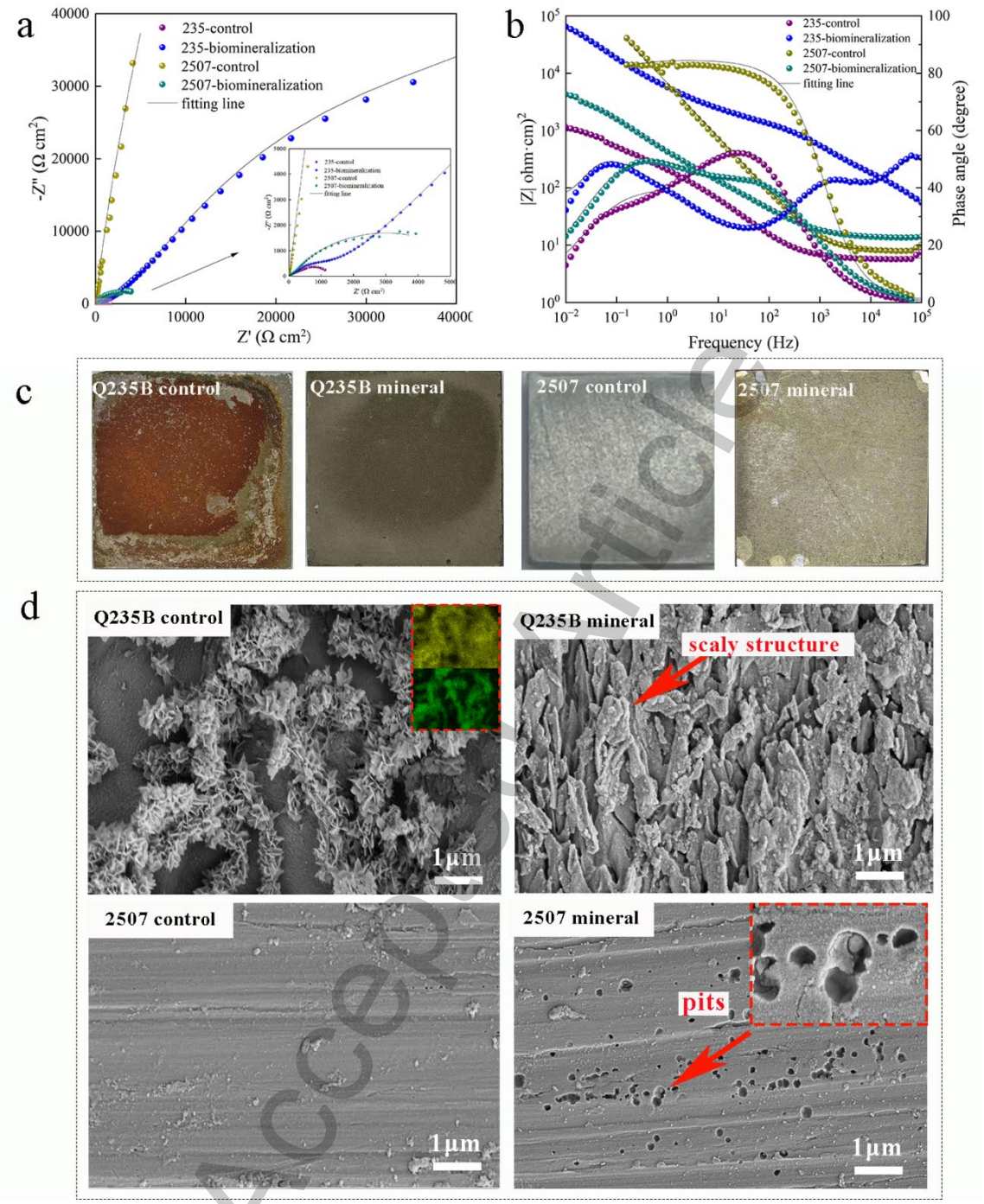

Fig 9. (a) Nyquist plot, (d) Bode plot after 3 d immersion, (c) macro images and (d)micro morphology of Q235B, 2507 immersed in ASW after 3 d with product removed.

Fig. 9 showed the Nyquist and Bode plots of bare steel and steel covered by the mature mineral layer immersed in simulated seawater after 3 d, which was described with $R_s(R_fQ_f)(R_{ct}Q_{dl})$ in Fig 6c. Q235B with the biomineral layer had a larger

capacitive loop and a clear diffusion feature. The film resistance (R_f) was approximately an order of magnitude higher than that of bare Q235B, the surface charge transfer process was inhibited (Tab. 2). The impedance modulus (|Z|) of biomineralized Q235B was also much higher than that of bare steel, indicating suppressed electrochemical reactions. The bare Q235B coupons showed one typical electrochemical process in the mid-frequency range, corrosion reaction was developed between substrates and seawater, with an oxide layer formed.

Pitting corrosion is one of the main causes leading to the failure of duplex stainless steel [51]. The EIS analysis on 2507 was the opposite, bare 2507 showed high impedance with a large capacitive loop and a phase angle of ~80-89°, behaving close to a capacitor and thus being less prone to corrosion. It represented the bare 2507 had outstanding corrosion resistance capacity because the surface Cr_2O_3 passive film was highly stable, the R_{ct} was ~2.0×10^5 Ω·cm² indicating that the surface hardly reacted with external ions in high salinity condition (Table 2). After the biomineral layer formed, the capacitive loop of 2507 became smaller, and both |Z| and the phase angle drop sharply, showing the damage by locally aggregated minerals to the passive film. mineral layer on 2507 induced by *P. spongiae* was thin and contained gaps, nonuniform regions could produce local stress and allowed Cl^- to touch substrates. Unmineralized regions could act as anodic sites (electron loss), leading to passive film breakdown.

Table 2. Electrochemical impedance parameters fitted from the Nyquist plots (Fig 9)

Groups	R_S (Ω·cm²)	Y_f (S.sⁿ/cm²)	n	R_f (Ω·cm²)	Y_{dl} (S.sⁿ/cm²)	n	R_{ct} (Ω·cm²)
Q235B control	5.8	2.7×10^{-2}	0.7	1134.0	9.1×10^{-4}	0.8	162.2
Q235Bmineralizati	1.0	7.2×10^{-5}	0.7	1.5×10	1.7×10^{-5}	0.6	2093.0

on				^{5}			
2507control	8.2	3.4×10^{-4}	0.8	100.5	2.4×10^{-5}	0.9	2.0×10^{5}
2507mineralization	13.2	7.5×10^{-4}	0.8	5737.0	7.1×10^{-4}	0.8	81.4

Fig. 9c showed the surface morphology of the bare steel and the protective layer after 3 d immersion in ASW. On the Q235B substrate, vigorous electrochemical activity was evident, leading to the formation of abundant yellow corrosion products adhered tightly and extensively to the surface. The corrosion products exhibited a characteristic flower-like morphology. By contrast, the biomineral layer effectively suppressed corrosion of Q235B, and no corrosion products were detected. After removing the biomineral layer, the underlying substrate displayed a scaly structure, which was possible related with the early stage bacterial activity (Fig. 9d). For 2507 stainless steel, the native passive film conferred remarkable corrosion resistance, allowing the substrate to retain metallic luster with without visible degradation. Nevertheless, the biomineral layer formed by *P. spongiae* disrupted the stability of the passive film, the uneaven biomineralized layer and accelerating electrochemical reaction resulted in pitting corrosion beneath the non-uniform biomineral coating. These pits were likely caused either by localized film rupture or by electron transfer effects during the biomineral layer formation. Overall, the biomineral layers induced by *P. spongiae* on different steel substrates exhibited varying efficiencies in mitigating high salinity corrosion, which are closely correlated with their structural characteristics.

The vast majority embryos in the blank control group developed and hatched normally, with no obvious mortality, confirmed that the experimental conditions were appropriate (Fig 10). In the positive control group, all embryos died within 24 h, consistent with acute toxicity induced by elevated Cu^{2+}, and no viable larvae were obtained, thereby validating the sensitivity of the assay. By contrast, embryos exposed to the biomineral leachates maintained high survival throughout the 3 d observation

period, the survival rate each time point remained at approximately 94-97%, and most embryos successfully hatched into active larvae (Fig 10). These results indicated that the biomineral coupons caused negligible adverse effects on early zebra fish and demonstrated favorable ecological safety under the tested conditions. Collectively, the findings suggested that the biomineralized layer can reduce surface reactivity while maintaining environmental compatibility, supported its potential application as an eco-friendly protective strategy for marine engineering.

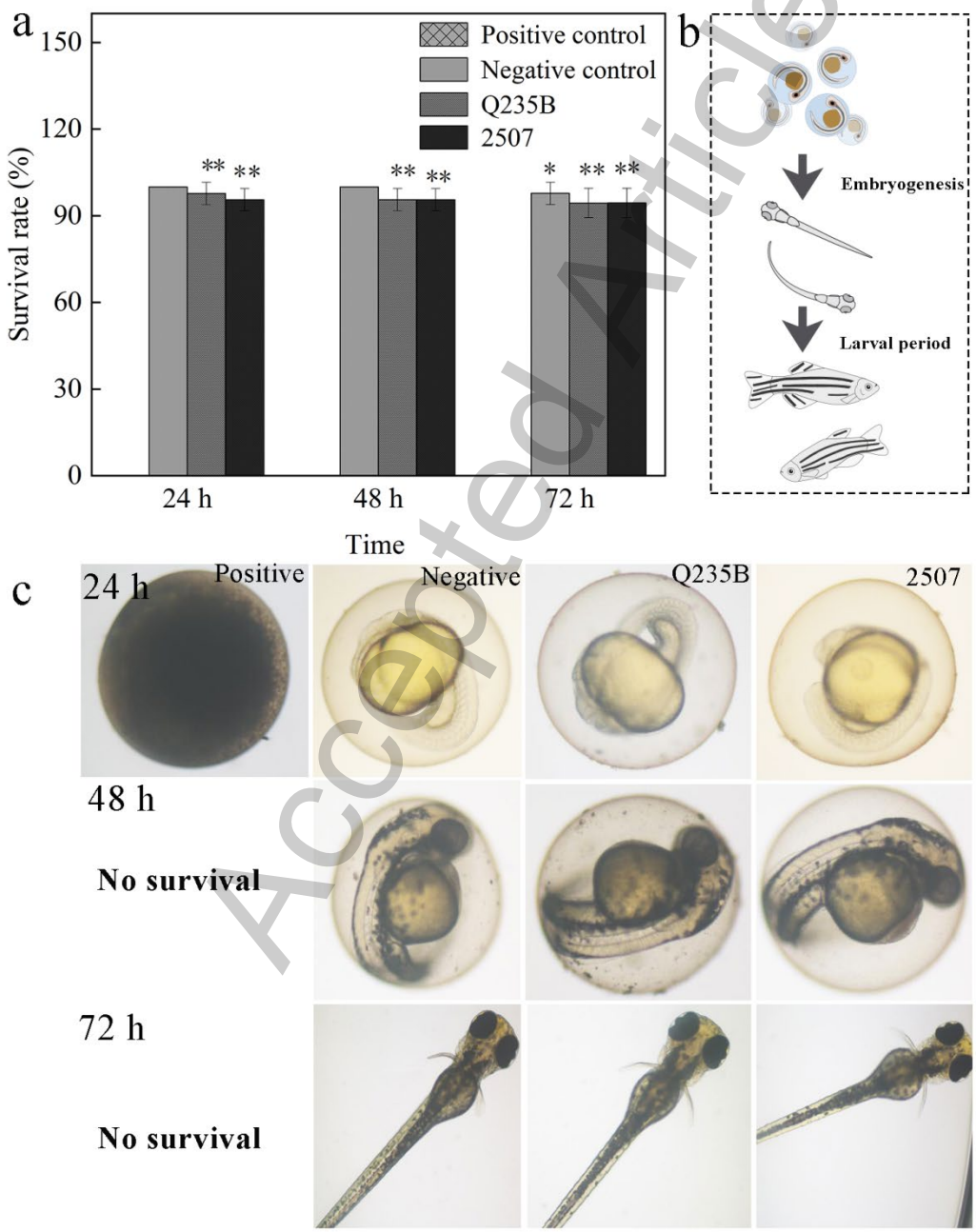

Fig 10. (a) The zebra fish survival rate with biomineral coupons, (b) the theoretical

growth process of zebra fish, (c) the actual growth of zebra fish with biomineral coupons (The statistical significance is *p<0.05, **p<0.01.).

Fig. 11 showed the formation process of biomineralization layers induced by *P. spongiae.* The biomineral layer on Q235B exhibited a dense and super-hydrophilic structure which was effectively inhibiting both corrosion and biofouling. Although the super-hydrophilic barrier formed on 2507 also suppressed biofouling, it adversely affected the integrity of passive film, leading to deterioration and pitting corrosion of stainless steel, it deserved a comprehensive investigation.

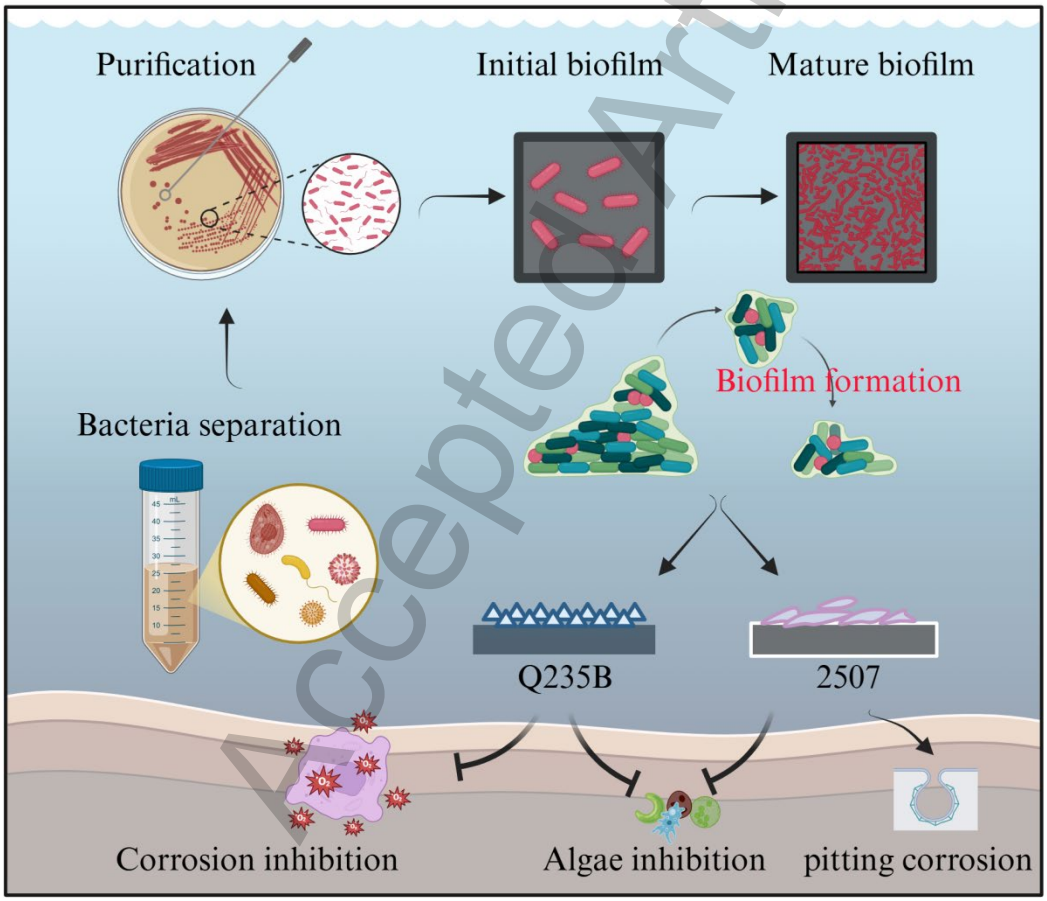

Fig 11. The formation process of biomineralization layers and their application in inhibiting corrosion and biofouling. This figure was created in BioRender. Sun, Z. (2026) https://BioRender.com/zio0x73.

CONCLUSION

This study aimed to evaluate the formation and functional performance of P. spongiae-induced biomineralized layers on Q235B carbon steel and 2507 stainless steel in artificial seawater. The results demonstrated that the biomineralization behavior and the protective performance of the formed layers were strongly dependent on the substrate. The biomineralized layer showed promising potential for suppressing corrosion and biofouling on carbon steel, while on stainless steel it mainly exhibited antifouling capability with limited corrosion protection. Overall, this work provides a basis for the future design and optimization of environmentally friendly biomineralization-based surface protection strategies for marine metallic materials.

DECLARATIONS

Authors' contributions

Yi Zhang conducted the experiments, analyzed the data, and wrote the manuscript. Zhenmei Sun and Yansheng Yin conceived the study, supervised the work, and revised the manuscript. Jiaxu Li, Xinyuan Wan, Gang Zhou, Canrong Lian, Rui Zhang, and Jinlin Lu assisted with the experiments, data collection, and manuscript revision. Jinwen Zhang provided funding support. All authors reviewed and approved the final manuscript.

Availability of data and materials

The data that support the findings of this study are available from the corresponding authors upon reasonable request.

AI and AI-assisted tools statement

The images of bacteria in the "separation and adhesion" and "biomineral coupons" section of the Graphic Abstract were sourced from the effect images generated by the author's AI guidance (ChatGPT 5.3 instant), while the rest of the images were drawn by the author themselves.

Financial support and sponsorship

This work was supported by the Guangdong Province Special Funding Project for the Development of Marine Economy under Grant No. GDNRC [2024] 41.

Conflicts of interest

All authors declared that there are no conflicts of interest.

Ethical approval and consent to participate

Not applicable.

Consent for publication

Not applicable.

REFERENCE

1. M. Wang, L.-H. Yang, H. Liu, X. Wang, W. Xu, H. Gao, C. Lin, Research on marine atmospheric corrosion behavior of carbon steel during Western Pacific voyage, J. Mater. Res. Technol., 36 (2025) 9678-9691. https://doi.org/10.2139/ssrn.5168090.

2. X. Yan, L. Yan, S. Kang, X. Qi, M. Xu, P. Zhang, Corrosion behavior and electrochemical corrosion of a high manganese steel in simulated marine splash zone, Mater. Res. Express, 8 (2021) 126507. https://doi.org/10.1088/2053-1591/ac3e96.

3. A. Wang, K. De Silva, M. Jones, W. Gao, Investigation of electrolysis corrosion on marine propellers, Mod. Phys. Lett., B 39 (2025) 2442011. https://doi.org/10.1142/S0217984924420119.

4. M.M.F. De Mesquita, M.A.C. Crapez, V.L. Teixeira, D.N. Cavalcanti, Potential interactions bacteria-brown algae, J. Appl. Phycol., 31 (2019) 867–883. https://doi.org/10.1007/s10811-018-1573-4.

5. J. Sun, X. Zhao, H. Rong, S. Yang, S. Wang, Z. An, Y. Li, X. Qu, Effect of *ochrobactrum sp*. on the corrosion behavior of 10MnNiCrCu steel in simulated marine environment, Int. J. Electrochem. Sci., 15 (2020) 2364–2374. https://doi.org/10.20964/2020.03.55.

6. D. Ariyanti, D.N. Sugianto, A. Purbasari, D. Lesdantina, E.P. Handayani, Synthesis of environmental-friendly fouling release coating, PDMS-X, to prevent the attachment of marine biofouling, J. Indian Chem. Soc., 102 (2025) 101768. https://doi.org/10.1016/j.jics.2025.101768.

7. G. Satasiya, M.A. Kumar, S. Ray, Biofouling dynamics and antifouling innovations: Transitioning from traditional biocides to nanotechnological interventions, Environ. Res., 269 (2025) 120943. https://doi.org/10.1016/j.envres.2025.120943.

8. D. Yang, Y. Huang, J. Li, Y. Gao, X. Zhao, W. Xu, Corrosion behavior of Q235B carbon steel in simulated seawater pumped storage system under operational conditions, J. Ocean. Limnol., 38 (2020) 1537–1547. https://doi.org/10.1007/s00343-020-0043-4.

9. M. Zhu, Q. Zhang, Y. Yuan, S. Guo, Y. Huang, Study on the correlation between passive film and AC corrosion behavior of 2507 super duplex stainless steel in simulated marine environment, J. Electroanal. Chem., 864 (2020) 114072. https://doi.org/10.1016/j.jelechem.2020.114072.

10. J. Chen, J. Liu, C. Zhou, F. Zhu, T. Chen, H. Zhang, An automatic image enhancement method based on the improved HCTLS, in: 2018 10 th IAPR workshop on pattern recognition in remote sensing (PRRS), IEEE, Beijing, (2018) 1–6. https://doi.org/10.1109/PRRS.2018.8486212.

11. Z. Sun, M. Moradi, Y. Chen, R. Bagheri, P. Guo, L. Yang, Z. Song, C. Xu, Simulation of the marine environment using bioreactor for investigation of 2507 duplex stainless steel corrosion in the presence of marine isolated *Bacillus Vietnamensis* bacterium, Mater. Chem. Phys., (2018) 149–156. https://doi.org/10.1016/j.matchemphys.2018.01.047.

12. H. Qiu, K. Feng, A. Gapeeva, K. Meurisch, S. Kaps, X. Li, L. Yu, Y.K. Mishra, R. Adelung, M. Baum, Functional polymer materials for modern marine biofouling

control, Prog. Polym. Sci., 127 (2022) 101516, https://doi.org/10.1016/j.progpolymsci.2022.101516.

13. J.-F. Päßler, E. Jarochowska, M. Bestmann, A. Munnecke, Distinguishing biologically controlled calcareous biomineralization in fossil organisms using electron backscatter diffraction (EBSD), Front. Earth Sci. 6 (2018) 16. https://doi.org/10.3389/feart.2018.00016.

14. T. Liu, Z. Guo, Z. Zeng, N. Guo, Y. Lei, T. Liu, S. Sun, X. Chang, Y. Yin, X. Wang, Marine bacteria provide lasting anticorrosion activity for steel via biofilm-induced mineralization, ACS Appl. Mater. Interfaces., 10 (2018) 40317–40327. https://doi.org/10.1021/acsami.8b14991.

15. N. Guo, Q. Zhao, X. Hui, Z. Guo, Y. Dong, Y. Yin, Z. Zeng, T. Liu, Enhanced corrosion protection action of biofilms based on endogenous and exogenous bacterial cellulose, Corros. Sci., 194 (2022) 109931. https://doi.org/10.1016/j.corsci.2021.109931.

16. Z. Guo, Q. Feng, N. Guo, Y. Yin, T. Liu, Positive effects of molybdenum on the biomineralization process on the surface of low-alloy steel catalyzed by Bacillus subtilis, Front. Microbiol. 15 (2024) 1428286.https://doi.org/10.3389/fmicb.2024.1428286.

17. Z. Guo, S. Pan, T. Liu, Q. Zhao, Y. Wang, N. Guo, X. Chang, T. Liu, Y. Dong, Y. Yin, Bacillus subtilis Inhibits Vibrio natriegens-Induced Corrosion via Biomineralization in Seawater, Front. Microbiol. 10 (2019) 1111. https://doi.org/10.3389/fmicb.2019.01111.

18. N. Kip, S. Jansen, M.F.A. Leite, M. De Hollander, M. Afanasyev, E.E. Kuramae, J.A.V. Veen, Methanogens predominate in natural corrosion protective layers on metal sheet piles, Sci. Rep., 7 (2017) 11899. https://doi.org/10.1038/s41598-017-11244-7.

19. X. Hao, Y. Bai, C. Ren, W. Chang, H. Qian, Y. Lou, L. Zhao, D. Zhang, X. Li, Self-healing effect of damaged coatings via biomineralization by Shewanella putrefaciens, Corros. Sci., 196 (2022) 110067. https://doi.org/10.1016/j.corsci.2021.110067.

20. M.J.F. Marques, J. Jaume, D. Mercier, A. Seyeux, S. Zanna, R. Basseguy, P. Marcus, The positive impact of biomineralization for marine corrosion protection of AA5083 alloy, Corros. Sci., 233 (2024) 112053. https://doi.org/10.1016/j.corsci.2024.112053.

21. H. Wang, X. Sun, Y. Wang, W. Shi, L. Wu, L. Miao, Marine steel protection based on biomineralization for sustainable development of coastal cities, Bioresour. Technol., 428 (2025) 132404. https://doi.org/10.1016/j.biortech.2025.132404.

22. M. Lv, M. Du, X. Zhao, Y. Du, Fundamental understanding of microbiologically influenced corrosion inhibition via biomineralization: A critical review, Crit. Rev. Environ. Sci. Technol., 55 (2025) 928–950. https://doi.org/10.1080/10643389.2025.2469860.

23. S. Guo, J. Jiang, D. Yang, H. Wu, Q. Xie, H. Liu, J. Chen, C. Ji, Microstructure evolution of Al-Zn-In-Mg-Ti sacrificial anodes during multi-pass equal-channel angular pressing and its impact on corrosion protection performance, Mater. Today Commun., 48 (2025) 113384. https://doi.org/10.1016/j.mtcomm.2025.113384.

24. R. Liu, Y. Guan, Y. Cui, F. Meng, F. Wang, L. Liu, The self-powered cathodic protection effect of flexible PDMS-based piezoelectric composites in a simulated pressure-alternating marine environment, Compos. Commun., 53 (2025). https://doi.org/10.1016/j.coco.2024.102166.

25. Y. Wu, W. Zhao, L. Wang, State of the art and current trends on the metal corrosion and protection strategies in deep sea, J. Mater. Sci. Technol., 215 (2025) 192–213. https://doi.org/10.1016/j.jmst.2024.07.026.

26. Z. Zhou, J. He, Y. Deng, X. Shi, Improving the protective performance of discrete Zn-based sacrificial anode by increasing porosity and alkali concentration of its encapsulation matrix. Cement. Concrete. Comp., 163 (2025) 106200. https://doi.org/10.1016/j.cemconcomp.2025.106200.

27. P. A. Vinagre, T. Simas, E. Cruz, E. Pinori, J. Svenson, Marine biofouling: a European database for the marine renewable energy sector, J. Mar. Sci. Eng., 8 (2020) 495. https://doi.org/10.3390/jmse8070495.

28. Y. Dong, G.-L. Song, J. Zhang, Y. Gao, Z.M. Wang, D. Zheng, Biocorrosion

induced by red-tide alga-bacterium symbiosis and the biofouling induced by dissolved iron for carbon steel in marine environment, J. Mater. Sci. Technol., 128 (2022) 107–117. https://doi.org/10.1016/j.jmst.2022.02.057.

29. W. He, H.-P. Xue, C. Liu, A.H. Zhang, J.-K. Huang, D.-F. Zhang, Biomineralization of struvite induced by indigenous marine bacteria of the genus *Alteromonas*, Front. Mar. Sci. 10 (2023) 1085345. https://doi.org/10.3389/fmars.2023.1085345.

30. N. Guo, Y. Wang, X. Hui, Q. Zhao, Z. Zeng, S. Pan, Z. Guo, Y. Yin, T. Liu, Marine bacteria inhibit corrosion of steel via synergistic biomineralization, J. Mater. Sci. Technol., 66 (2021) 82–90. https://doi.org/10.1016/j.jmst.2020.03.089.

31. S. Beurmann, B. Ushijima, C.M. Svoboda, P. Videau, A.M. Smith, S.P. Donachie, G.S. Aeby, S.M. Callahan, *Pseudoalteromonas piratica* sp. nov., a budding, prosthecate bacterium from diseased Montipora capitata, and emended description of the genus *Pseudoalteromonas*, Int. J. Syst. Evol. Microbiol., 67 (2017) 2683–2688. https://doi.org/10.1099/ijsem.0.001995.

32. K. Zheng, Y. Dong, Y. Liang, Y. Liu, X. Zhang, W. Zhang, Z. Wang, H. Shao, Y.Y. Sung, W.J. Mok, L.L. Wong, A. McMinn, M. Wang, Genomic diversity and ecological distribution of marine *Pseudoalteromonas phages*, Mar. Life. Sci. Technol., 5 (2023) 271–285. https://doi.org/10.1007/s42995-022-00160-z.

33. P. Saravanan, S. Jayachandran, Preliminary characterization of exopolysaccharides produced by a marine biofilm-forming bacterium *Pseudoalteromonas ruthenica* (SBT 033): EPS produced by *P. ruthenica*, Lett. Appl. Microbiol., 46 (2007) 1–6. https://doi.org/10.1111/j.1472-765X.2007.02215.x.

34. L. Hao, W. Liu, K. Liu, K. Shan, C. Wang, C. Xi, J. Liu, Q. Fan, X. Zhang, X. Lu, Y. Xu, R. Cao, Y. Ma, L. Zheng, B. Cui, Isolation, Optimization of fermentation conditions, and characterization of an exopolysaccharide from *Pseudoalteromonas agarivorans* Hao 2018, Mar. Drugs., 17 (2019) 703. https://doi.org/10.3390/md17120703.

35. B. Colin, J. Vincent, L. Koziorowszki, A. Frein, I. Lanneluc, R. Sabot, P. Refait, S. Sablé, M. Jeannin, Calcareous deposit formation under cathodic polarization and

marine biocalcifying bacterial activity, Bioelectrochemistry 148 (2022) 108271. https://doi.org/10.1016/j.bioelechem.2022.108271.

36. N. Torres-Crespo, F. Martínez-Ruiz, M.T. González-Muñoz, E.J. Bedmar, G.J. De Lange, F. Jroundi, Role of bacteria in marine barite precipitation: A case study using Mediterranean seawater, Sci. Total Environ., 512–513 (2015) 562–571. https://doi.org/10.1016/j.scitotenv.2015.01.044.

37. S.J. Kim, B.-G. Kim, H.J. Park, J.H. Yim, Cryoprotective properties and preliminary characterization of exopolysaccharide (P-Arcpo 15) produced by the Arctic bacterium *Pseudoalteromonas elyakovii* Arcpo 15, Prep. Biochem. Biotech., 46 (2016) 261–266. https://doi.org/10.1080/10826068.2015.1015568.

38. G.Z. Moldabayeva, A.L. Kozlovskiy, E.I. Kuldeyev, A.K. Syzdykov, A. Bakesheva, Study of the effectiveness of corrosion resistance growth by application of layered AlN–TiO2 coatings, Coatings 14 (2024) 373. https://doi.org/10.3390/coatings14040373.

39. Z. Zhang, N. Zhao, F. Qi, B. Zhang, B. Liao, X. Ouyang, Reinforced superhydrophobic anti-corrosion epoxy resin coating by fluorine–silicon–carbide composites, Coatings 10 (2020) 1244. https://doi.org/10.3390/coatings10121244.

40. H. Liu, W. Chen, Y. Tan, G. Meng, H. Liu, Yf. Cheng, H. Liu, Characterizations of the biomineralization film caused by marine *Pseudomonas stutzeri* and its mechanistic effects on X80 pipeline steel corrosion, J. Mater. Sci. Technol., 125 (2022) 15–28. https://doi.org/10.1016/j.jmst.2022.02.033.

41. M. Li, H. Wu, Y. Sun, Corrosion performance of welded joints for E40 marine steel, Metals 13 (2023) 1528. https://doi.org/10.3390/met13091528.

42. J. Alcántara, D.D.L. Fuente, B. Chico, J. Simancas, I. Díaz, M. Morcillo, Marine atmospheric corrosion of carbon steel: a review, Materials 10 (2017) 406. https://doi.org/10.3390/ma10040406.

43. X. Wang, R.E. Melchers, Corrosion of carbon steel in presence of mixed deposits under stagnant seawater conditions, J. Loss Prev. Process Ind., 45 (2017) 29–42. https://doi.org/10.1016/j.jlp.2016.11.013.

44. H. Singh, Y. Xiong, E. Rani, S. Wang, M. Kharbach, T. Zhou, H. Yao, Y. Niu, A.

Zakharov, G. King, F.M.F. De Groot, J. Kömi, M. Huttula, W. Cao, Unveiling nano-scaled chemical inhomogeneity impacts on corrosion of Ce-modified 2507 super-duplex stainless steels, Npj Mater. Degrad., 6 (2022) . https://doi.org/10.1038/s41529-022-00263-z.

45. H. Chen, H. Cui, G. Ma, H. Zhang, Y. Zhu, X. Song, Mechanical and corrosion behavior of oscillating laser beam welded 2507 super duplex stainless steel: Synergistic effects of acidic seawater and strain states, J. Mater. Sci. Technol., 251 (2026) 227–240. https://doi.org/10.1016/j.jmst.2025.07.010.

46. T. Zhao, L. He, Z. Qiu, Z. Zhang, C. Lin, Synergistic effect between sulfate-reducing bacteria and *Shewanella algae* on corrosion behavior of 321 stainless steel, J. Mater. Res. Technol., 26 (2023) 4906–4917. https://doi.org/10.1016/j.jmrt.2023.08.237.

47. T. Cui, H. Qian, W. Chang, H. Zheng, D. Guo, C.T. Kwok, L.M. Tam, D. Zhang, Towards understanding *Shewanella algae*-induced degradation of passive film of stainless steel based on electrochemical, XPS and multi-mode AFM analyses, Corro. Sci. 218 (2023) 111174. https://doi.org/10.1016/j.corsci.2023.111174.

48. X. Wang, J. Liu, W. Zhao, J. Liu, J. Liang, F. Thompson, X.-H. Zhang, Fine-scale structuring of planktonic *Vibrio* spp. in the Chinese Marginal Seas, Appl Environ Microbiol 88 (2022) e01262-22. https://doi.org/10.1128/aem.01262-22.

49. S. Liu, C. Dong, Y. Zhu, Z. Wang, Y. Li, G. Feng, Recent Developments on biomineralization for erosion control, Appl. Sci., 15 (2025) 6591. https://doi.org/10.3390/app15126591.

50. S. Reiprich, E. Akova, A. Aszódi, V. Schönitzer, Hyaluronan synthases' expression and activity are induced by fluid shear stress in bone marrow-derived mesenchymal dtem cells, IJMS 22 (2021) 3123. https://doi.org/10.3390/ijms22063123.

51. M Liu, C Du, Z. Liu, L Wang, R Zhong, X Cheng, J Ao, T Duan, Y Zhu, X li. A review on pitting corrosion and environmentally assisted cracking on duplex stainless steel, Microstructures., (2023) 3: 2023020. https://doi.org/10.20517/microstructures.2023.02.